

For example, over large intervals of temperature noncompensating changes in viscosity and molecular extension might cause discernable changes in the

Brownian diffusion and hence require the use of a "limiting breadth" which itself is a function of temperature.

## QUANTUM RESONANCES IN THE AMPLIFICATION OF ULTRASOUND IN BISMUTH

K. Walther

Philips Research Laboratories Hamburg, Hamburg-Stellingen, Germany

(Received 28 December 1965)

In this Letter experimental evidence is presented of ultrasonic amplification in bismuth subjected simultaneously to an electric and a magnetic field. Recently, an increase of 14 dB/cm in the amplitude of a 15-Mc/sec shear wave in bismuth with application of an electric drift field was reported.<sup>1</sup> However, it was not evident whether this figure represents a net gain in the electronic part of the ultrasonic interaction. In what follows, we have proven the existence of ultrasonic gain by observing "inverted" giant quantum oscillations, i.e., the maxima of ultrasonic attenuation<sup>2</sup> are converted into minima by the application of a suitable electric field. Estimated values of the de-attenuation caused by the electric drift field range around 85 dB/cm, the "net" gain referred to the attenuation at zero magnetic field being 18 dB/cm, at 223 Mc/sec.

The present experiment was carried out at 4.2°K with a single crystal of pure bismuth (resistance ratio  $\rho_{300^\circ\text{K}}/\rho_{4.2^\circ\text{K}} = 140$ ). The sample dimensions are  $1.407 \times 0.389 \times 0.680$  cm<sup>3</sup>, along the respective edge directions  $\hat{\xi}$ ,  $\hat{\eta}$ ,  $\hat{\zeta}$  as given in Table I. The electric field  $\vec{E}$  is applied along  $\hat{\xi}$ , the wave normal  $\hat{q}$  of the ultrasound along  $\hat{\zeta}$ , and the magnetic field  $\vec{B}$  can be rotated in the  $\hat{\xi}$ - $\hat{\eta}$  plane. Ultrasonic waves were generated and received by Y-cut quartz transducers (fundamental frequency 20 Mc/sec) with the direction of polarization along  $\hat{\xi}$ . We observed a longitudinal wave  $L$  and two shear waves  $S_1$ ,  $S_2$  with apparent velocities of  $(2.14, 0.96, \text{ and } 0.83) \times 10^5$  cm/sec, respectively, whereas the values calculated from the elas-

tic constants<sup>3</sup> are  $(2.12, 1.37, \text{ and } 1.04) \times 10^5$  cm/sec, respectively. The strong discrepancy of the shear wave velocities may be due to boundary reflections caused by the large deviations ( $\approx 34^\circ$ ) between wave normal and direction of energy flux.<sup>4</sup> The mode  $L$  shows virtually no magnetoacoustic electronic interaction;  $S_1$  is slightly and  $S_2$  very strongly affected. The measurements described below refer to mode  $S_2$  with  $\angle(\vec{E}, \vec{B}) = \Theta = 56^\circ$ .

Figure 1 shows the received amplitude of  $S_2$  at 188 Mc/sec as a function of the magnetic field strength. In curve  $b$  no electric drift field

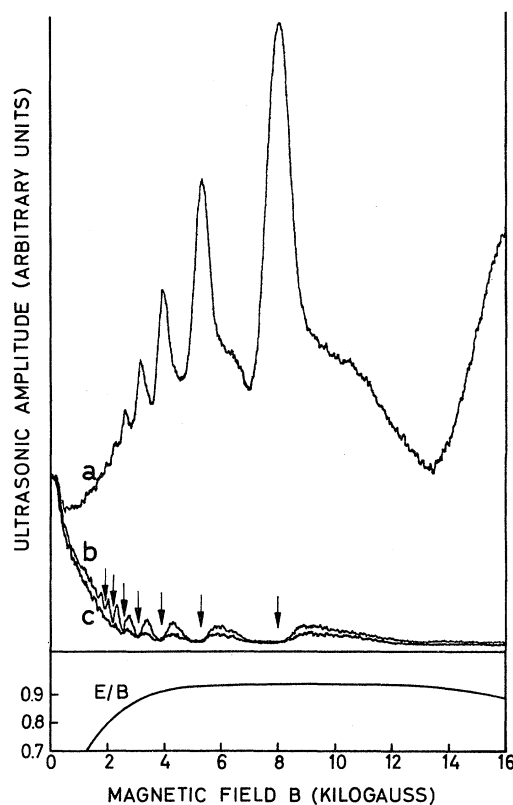


FIG. 1. Received amplitude of shear wave  $S_2$  at 188 Mc/sec in bismuth as a function of magnetic field strength.  $a$ ,  $\vec{B}$  "normal," drift field applied;  $b$ ,  $\vec{B}$  "normal," without drift field;  $c$ ,  $\vec{B}$  "reverse," drift field applied. Lower curve:  $E/B$  in units of  $10^5$  cm/sec.

Table I. Components of the unit edge vectors  $\hat{\xi}$ ,  $\hat{\eta}$ ,  $\hat{\zeta}$  in the crystallographic coordinate system:  $x$ =binary axis,  $y$ =bisectrix,  $z$ =trigonal axis.

	$\hat{\xi}$	$\hat{\eta}$	$\hat{\zeta}$
$x$	-0.492	-0.848	+0.180
$y$	-0.636	+0.495	+0.580
$z$	+0.592	-0.195	+0.794

is present. The positions of maximum ultrasonic attenuation can be determined more accurately from measurements at 102 Mc/sec and are marked by arrows. In curve *a* an electric drift field (pulse length 12  $\mu$ sec) is applied such that the carriers drift in the direction of sound propagation ( $\vec{B}$  "normal"). The drift current was adjusted for optimum amplification conditions above the kink point.<sup>5</sup> Evidently the quantum resonance pattern becomes inverted; i.e., the positions of peak amplification correspond to attenuation maxima (arrows) at  $E=0$ . This behavior was predicted previously on theoretical grounds.<sup>6</sup> In curve *c* the direction of carrier drift is opposite to the direction of wave propagation ( $\vec{B}$  "reverse") causing an increase of the ultrasonic attenuation. The bottom curve shows that in the range  $B=3$  to 16 kG the amplification and the attenuation are portrayed as a function of magnetic field under conditions of almost constant carrier drift velocity<sup>7</sup>  $\vec{v}_D = (\vec{E} \times \vec{m} \cdot \vec{B}) / (\vec{B} \cdot \vec{m} \cdot \vec{B})$ , where  $\vec{m}$  is the effective mass tensor.

A cyclotron effective mass  $m_c \approx 0.01m_0$  is evaluated (neglecting "tilt" effect) from the measured period of quantum oscillations,  $\Delta(1/B) = 6.56 \times 10^{-5} \text{ G}^{-1}$ . With the magnetic field direction used, two of the three electron ellipsoids have small cyclotron masses  $m_c = 0.0092m_0$  and  $m_c = 0.010m_0$ , as calculated from the mass-tensor components of Reneker.<sup>8</sup> The respective values of projected drift velocity are  $\vec{v}_D \cdot \hat{q} = 1.1E/B$  and  $0.62E/B$ . Therefore, only one ellipsoid satisfies the condition of amplification<sup>7</sup>  $\vec{v}_D \cdot \hat{q} \geq v_s$  for the drift fields used in this experiment.

Figure 2 shows the ultrasonic attenuation  $\Gamma - \Gamma_0$  as a function of the projected drift velocity  $\vec{v}_D \cdot \hat{q} = 1.1E/B$  for various frequencies. The magnetic field strength is held fixed at  $B=8$  kG corresponding to a quantum resonance peak (see Fig. 1).  $\Gamma_0$  is the attenuation with  $E=0$  and  $B=0$ . The current density is plotted with the same abscissa and exhibits a rather "soft" kink<sup>5</sup> around  $\vec{v}_D \cdot \hat{q} = 0.8 \times 10^5 \text{ cm/sec}$ , coinciding approximately with the crossover region  $\Gamma - \Gamma_0 = 0$  and the apparent sound velocity of  $S_2$ . A maximum ultrasonic amplification  $\Gamma - \Gamma_0 = -18 \text{ dB/cm}$  was obtained at 223 Mc/sec with a drift velocity around  $1 \times 10^5 \text{ cm/sec}$ ; the maximum change of ultrasonic signal level due to the electric drift field was extrapolated to be 85 dB/cm in this case. An over-all ultrasonic gain was not obtained since the attenuation  $\Gamma_0$

is very high (estimated value at 223 Mc/sec,  $\Gamma_0 = 75 \text{ dB/cm}$ ). The question as to the size of the electronic contribution to  $\Gamma_0$  is still open. Moreover, only part of the electronic interaction is associated with electron-phonon drag<sup>9</sup> and can therefore contribute to the amplification process.

Theoretically<sup>6</sup> the ultrasonic attenuation as a function of drift velocity should be antisymmetric around the point  $\vec{v}_D \cdot \hat{q} = v_s$ . The decrease of ultrasonic amplification for drift velocities larger than  $1 \times 10^5 \text{ cm/sec}$  is not explained by this theory and may be caused by two effects: (i) Hot-electron effects may reduce ultrasonic gain.<sup>10</sup> Under conditions of strong mutual electron-phonon drag, the heating of electrons is small for drift velocities below the kink point<sup>11</sup> and increases rapidly beyond that point. (ii) Non-linear interaction with ultrasonic noise generated by the drifting carriers may cause a strong reduction of the amplification of an external signal, as is well known for CdS.<sup>12</sup> Strong interaction is favored by the fact, supported by direct observation in bismuth,<sup>13</sup> that signal and noise are both confluent with the carrier drift. The generation of noise is strongly dependent on the orientation of the magnetic field,<sup>13</sup> and it was found that minimum noise generation corresponds to optimum signal amplification,

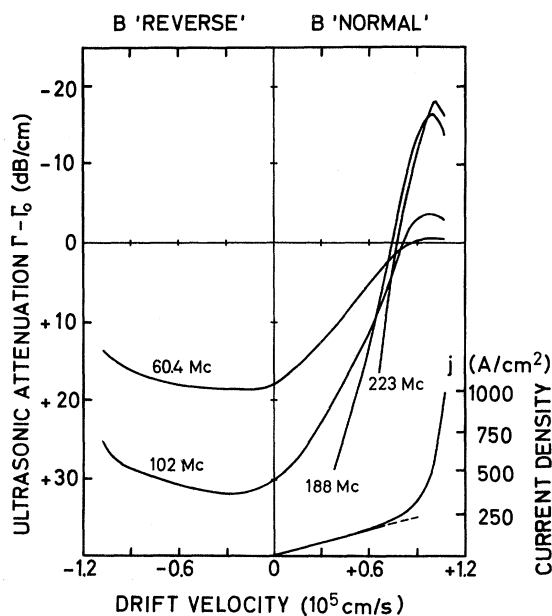


FIG. 2. Ultrasonic attenuation  $\Gamma - \Gamma_0$  of shear wave  $S_2$ , and current density  $j$ , in bismuth as a function of projected electron drift velocity  $v_D \cdot \hat{q} = 1.1E/B$ , in a magnetic field of  $B=8$  kG.

and vice versa. Accordingly, the angle  $\Theta = 56^\circ$  stated above was chosen for optimum signal gain, and build-up of noise was barely detectable in this case. The rather skew sample geometry (see Table I) was chosen deliberately, since the amplification effects are considerably larger than with other more symmetric arrangements (e.g.,  $\hat{q} \parallel y$  or  $\hat{q} \parallel z$ ), although in the latter case the mode of ultrasonic propagation may be easier to interpret, because the deviations between wave normal and direction of energy flux are smaller or even zero.

Stimulating discussions with K. J. Schmidt-Tiedemann, as well as technical assistance by D. Restorff and W. Funk, are gratefully acknowledged.

<sup>1</sup>A. M. Toxen and S. Tansal, Phys. Rev. Letters 10,

481 (1963).

<sup>2</sup>A. M. Toxen and S. Tansal, Phys. Rev. 137, A211 (1965).

<sup>3</sup>Y. Eckstein, A. W. Lawson, and D. H. Reneker, J. Appl. Phys. 31, 1534 (1960).

<sup>4</sup>S. Epstein and A. P. de Bretteville, Phys. Rev. 138, A771 (1965).

<sup>5</sup>L. Esaki, Phys. Rev. Letters 8, 4 (1962).

<sup>6</sup>R. F. Kazarinov and V. G. Skobov, Zh. Eksperim. i Teor. Fiz. 43, 1496 (1962) [translation: Soviet Phys.-JETP 16, 1057 (1963)]; H. N. Spector, Phys. Rev. 132, 522 (1963).

<sup>7</sup>S. G. Eckstein, Phys. Letters 13, 30 (1964).

<sup>8</sup>D. H. Reneker, Phys. Rev. 115, 303 (1959).

<sup>9</sup>T. Yamada, J. Phys. Soc. Japan 20, 1424 (1965).

<sup>10</sup>E. M. Conwell, Proc. IEEE 52, 964 (1964).

<sup>11</sup>V. P. Kalashnikov, Fiz. Tverd. Tela 6, 2435 (1964) [translation: Soviet Phys.-Solid State 6, 1931 (1965)].

<sup>12</sup>J. H. McFee, J. Appl. Phys. 34, 1548 (1963).

<sup>13</sup>K. Walther, Phys. Rev. Letters 15, 706 (1965).

## ELECTROREFLECTANCE IN AlSb: OBSERVATION OF THE DIRECT BAND EDGE\*

Manuel Cardona, Fred H. Pollak, and Kerry L. Shaklee

Physics Department, Brown University, Providence, Rhode Island  
(Received 3 March 1966)

We have determined the direct band edge of AlSb (2.218 eV) from its electroreflectance<sup>1,2</sup> spectrum at room temperature. This edge is obscured by indirect transitions in conventional optical measurements.<sup>3</sup> The knowledge of this direct band gap, which corresponds to transitions between the  $\Gamma_{15}$  valence band and the lowest  $\Gamma_1$  conduction band, is very important for energy-band calculations with adjustable parameters.<sup>4,5</sup> We have also observed in the electroreflectance spectrum the  $E_1$  transitions ( $\Lambda_3-\Lambda_1$ ) and their spin-orbit splitting  $\Delta_1$ , the  $E_0'$  transitions ( $\Delta_3-\Delta_4$ ,  $\Delta_1$ ) and their spin-orbit splitting  $\Delta_0'$ , and the  $E_2$  transitions ( $X_5-X_1$ ,  $X_3$ ) with their splitting  $\delta$  due to the lack of inversion symmetry in zinc blende.

The electrolytic method of measuring electroreflectance<sup>2</sup> is particularly suitable to AlSb provided one uses a nonaqueous electrolyte. Good quality AlSb chemically polished surfaces cannot be easily prepared since this material reacts with the water vapor present in the air. Surfaces suitable for electroreflectance measurements can be prepared by cleaving the material inside the electrolyte. We used as electrolyte a KCl solution in methanol. The cleaved AlSb surfaces remain untarnished for several hours in such a solution.

Figure 1 shows the electroreflectance spectrum of *p*-type AlSb at room temperature. The sign of  $\Delta R$  is that observed for an increase in the surface field (internal field plus modulating field). No signal is seen around the indirect absorption edge (1.6 eV). The lowest energy structure appears around 2.2 eV. Sim-

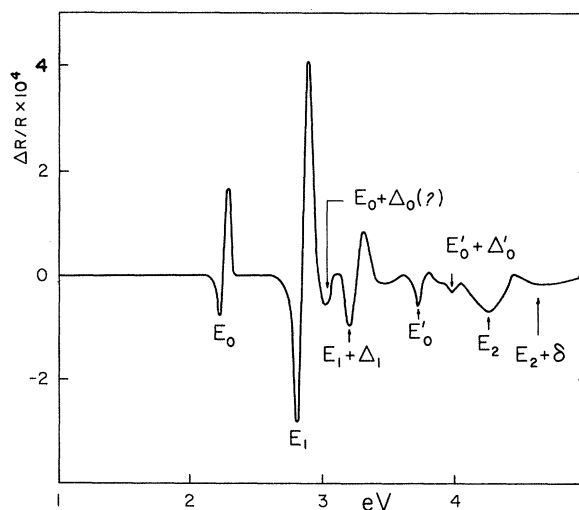


FIG. 1. Electroreflectance spectrum of *p*-type AlSb at room temperature.  $V_{ac} = 16$  V peak to peak,  $V_{dc} = 4$  V.